

***Ab-initio* self-energy corrections in systems with metallic screening**

Marco Cazzaniga,* Nicola Manini, Luca Guido Molinari, and Giovanni Onida

*Physics Department, Università degli Studi di Milano, I-20133 Milan (Italy)**European Theoretical Spectroscopy Facility (ETSF)*

(Dated: November 20, 2007)

Abstract

The calculation of self-energy corrections to the electron bands of a metal requires the evaluation of the intraband contribution to the polarizability in the small- \mathbf{q} limit. When neglected, as in standard *GW* codes for semiconductors and insulators, a spurious gap opens at the Fermi energy. Systematic methods to include intraband contributions to the polarizability exist, but require a computationally intensive Fermi-surface integration. We propose a numerically cheap and stable method, based on a fit of the power expansion of the polarizability in the small- \mathbf{q} region. We test it on the homogeneous electron gas and on real metals such as sodium and aluminum.

PACS numbers: 71.15.-m, 71.38.Cn, 71.20.-b, 71.15.Dx,

*Electronic address: marco.cazzaniga@unimi.it

I. INTRODUCTION

More than 20 years of successful applications have established Hedin's *GW* approach [1, 2] and its numerical implementations [3, 4] as the state-of-the-art and most widely used theoretical method for *ab-initio* bandstructure calculations including self-energy effects. Efficient algorithms have been devised to encompass the major numerical bottlenecks in such calculations, e.g. by avoiding \mathbf{k} -space convolutions by a space-time method [5], or avoiding summations over empty states in the evaluation of the polarizability [6, 7], or using localized basis functions [8], and/or model screening functions [9, 10, 11]. Several computer codes have been devised for *ab-initio GW* calculations, and are presently available, often under public domain [12, 13, 14]. However, systems with metallic screening present an additional, numerically challenging, difficulty: in the evaluation of the \mathbf{k} -space integrals for the intraband contribution to the electron screening, the contribution of the Fermi surface can dramatically slow down the convergence with respect to the \mathbf{k} -space sampling. As a consequence, the possibility to perform such *ab-initio GW* calculations in gapless systems with a large unit cell is hindered. Even worse, when calculations are performed with standard computer codes, unconverged \mathbf{k} -point sampling gives rise to a spurious gap at the Fermi level. The gap vanishes only in the limit of infinitely dense sampling, and is shown to close very slowly as the number of \mathbf{k} -points increases. Solutions based on explicit Fermi surface integration [15, 16, 17] are effective but result in cumbersome coding and substantial increase of computation time.

In this paper we present a numerically stable and efficient method, based on a Taylor expansion of the polarizability matrix in the small- \mathbf{q} region, which includes intraband contributions and avoids explicit Fermi-surface calculations. The method has been implemented successfully into the `abinit` [12, 18] package, and is shown to remove the spurious gap at the Fermi level already with a limited number of \mathbf{k} -points. Results are presented for the homogeneous electron gas (HEG) as well as for real metals such as Na and Al.

This paper is organized as follows: in Sec. II we briefly review the standard *GW* scheme and describe the difficulties that arise when it is applied to metals naively. In Sec. III we analyze the origin of the problem, and propose our solution in Sec. IV. In Sec. V we test the method on different metallic systems, and we discuss the results in Sec. VI.

II. THEORETICAL FRAMEWORK

The present work deals with the many-body problem in the standard Hedin's scheme based on the following set of self-consistent equations [1]:

$$G(1, 2) = G_0(1, 2) + \int G_0(1, 3)\Sigma(3, 4)G(4, 2) d3d4 \quad (1)$$

$$\Gamma(1, 2; 3) = \delta(1, 2)\delta(1, 3) + \int \frac{\delta\Sigma(1, 2)}{\delta G(4, 5)}G(4, 6)G(7, 5)\Gamma(6, 7; 3) d4d5d6d7 \quad (2)$$

$$\chi(1, 2) = -i \int G(1, 3)G(4, 1)\Gamma(3, 4; 2) d3d4 \quad (3)$$

$$W(1, 2) = v_C(1, 2) + \int v_C(1, 3)\chi(3, 4)W(4, 2) d3d4 \quad (4)$$

$$\Sigma(1, 2) = i \int G(1, 3)W(4, 1)\Gamma(3, 2; 4) d3d4, \quad (5)$$

G and G_0 are the exact and Hartree's Green functions for the electron, v_C is the bare Coulomb interaction, W is the screened potential, χ is the electric polarizability, Σ is the self energy, and Γ is the vertex function. An argument such as "1" stands for the set of position, time and spin variables $(\mathbf{r}_1, t_1, \sigma_1)$. Equations (1-5) constitute a formally closed set of equations for the five correlators. The functional derivative in Eq. (2) provides the vertex corrections and is a formidable computational difficulty. The most important approximation that is usually made is to neglect the vertex entirely and put $\Gamma(1, 2; 3) = \delta(1, 2)\delta(1, 3)$ in the remaining four equations. This explains the name GW , since Eq. (5) now simplifies to the product

$$\Sigma(1, 2) = iG(1, 2)W(2, 1). \quad (6)$$

A GW calculation proceeds as follows. One assumes initially $\Sigma = 0$, $G = G_0$ in Eq. (1). Next, one determines $\chi = \chi_0$ through Eq. (3) with $\Gamma = 1$, and computes W from Eq. (4). The first estimate of Σ is obtained in Eq. (6), and can be used to update G and the other correlators. This procedure can be iterated until self-consistency is reached. However, several non-selfconsistent GW approaches are possible [19]. In the present work, we choose to perform calculations within the so-called G_0W_0 approximation [3, 4], which stops the iteration without updating G and W . One first evaluates the independent-particle polarizability

$$\chi_0(1, 2) = -i G_0(1, 2) G_0(2, 1) \quad (7)$$

and the dielectric function

$$\epsilon(1, 2) = \delta(1, 2) - \int v_C(1, 3) \chi_0(3, 2) d3d4, \quad (8)$$

which provides the solution of Eq. (4), $W_0(1, 2) = \int \epsilon^{-1}(1, 3) v_C(3, 2) d3$, and the self energy $\Sigma(1, 2) = iG_0(1, 2)W_0(2, 1)$. This approximation is usually a successful one, while self-consistent GW has been shown to lead to a worse treatment of electron correlations in prototypical systems such as the HEG (where it gives a bandwidth larger than the DFT one [20]) and solid silicon (where the band gap turns out even larger than experiment [21]). The simpler G_0W_0 approach leads typically to a 10% bandwidth reduction with respect to DFT, in better agreement with experiment, thus suggesting a partial cancellation of errors due to lack of self-consistency and of vertex corrections in [22, 23].

In the G_0W_0 approximation, one can start from a DFT-LDA electronic-structure calculation. The quasiparticle energies E_j are hence evaluated as first order corrections to the Kohn-Sham (KS) eigenvalues ϵ_j , with respect to the perturbation $(\Sigma - V_{XC})$, and by linearizing the energy dependence of Σ [3, 4]:

$$E_j \simeq \epsilon_j + \frac{\langle \Sigma(\epsilon_j) - V_{XC} \rangle}{1 - \left\langle \frac{\partial \Sigma(\omega)}{\partial \omega} \right\rangle_{\omega=\epsilon_j}}. \quad (9)$$

Expectation values are taken on the corresponding KS state $|\mathbf{k}, j\rangle$; the denominator is the quasiparticle weight. One of the heaviest parts of the G_0W_0 computation is the inversion of the symmetrized dielectric matrix, which in reciprocal space reads:

$$\epsilon_{\mathbf{G}, \mathbf{G}'}(\mathbf{q}, \omega) = \delta_{\mathbf{G}, \mathbf{G}'} - 4\pi \frac{1}{|\mathbf{q} + \mathbf{G}|} \chi_{0 \mathbf{G}, \mathbf{G}'}(\mathbf{q}, \omega) \frac{1}{|\mathbf{q} + \mathbf{G}'|}. \quad (10)$$

The inversion must be performed on a mesh of frequencies spanning a range significantly wider than the range of interest for the bandstructure.

The inverse dielectric matrix leads immediately to the effective screened potential:

$$W_{\mathbf{G}, \mathbf{G}'}(\mathbf{q}, \omega) = 4\pi \frac{1}{|\mathbf{q} + \mathbf{G}|} \epsilon_{\mathbf{G}, \mathbf{G}'}^{-1}(\mathbf{q}, \omega) \frac{1}{|\mathbf{q} + \mathbf{G}'|}. \quad (11)$$

A great simplification can be achieved by introducing an additional plasmon-pole approximation, where the frequency dependence of each \mathbf{G}, \mathbf{G}' matrix element is parameterized by:

$$\epsilon_{\mathbf{G}, \mathbf{G}'}^{-1}(\mathbf{q}, \omega) = \delta_{\mathbf{G}, \mathbf{G}'} + \frac{\Omega_{\mathbf{G}, \mathbf{G}'}^2(\mathbf{q})}{\omega^2 - \tilde{\omega}_{\mathbf{G}, \mathbf{G}'}^2(\mathbf{q})}. \quad (12)$$

The parameters $\Omega_{\mathbf{G},\mathbf{G}'}^2(\mathbf{q})$ and $\tilde{\omega}_{\mathbf{G},\mathbf{G}'}^2(\mathbf{q})$ are determined by evaluating the polarizability $\chi_{0\mathbf{G},\mathbf{G}'}(\mathbf{q},\omega)$ only at two values of the frequency, usually at $\omega = 0$ and at a purely imaginary frequency of the magnitude of the plasma frequency $\omega = i\omega_P$. In the following we adopt this plasmon-pole model, since the difficulties related to the small wave-vector screening would occur identically if the detailed ω dependence of ϵ^{-1} were considered.

The polarizability χ_0 is given by the standard expression [24, 25]

$$\chi_{0\mathbf{G},\mathbf{G}'}(\mathbf{q},i\omega) = -\frac{2}{V_{BZ}} \sum_{j,j'} \int_{BZ} d^3k \frac{f(\epsilon_{j'}(\mathbf{k}+\mathbf{q})) - f(\epsilon_j(\mathbf{k}))}{i\omega - [\epsilon_{j'}(\mathbf{k}+\mathbf{q}) - \epsilon_j(\mathbf{k})]} \langle \mathbf{k}, j | e^{-i(\mathbf{q}+\mathbf{G})\cdot\hat{\mathbf{r}}} | \mathbf{k} + \mathbf{q}, j' \rangle \langle \mathbf{k} + \mathbf{q}, j' | e^{i(\mathbf{q}+\mathbf{G}')\cdot\hat{\mathbf{r}}} | \mathbf{k}, j \rangle, \quad (13)$$

where $f(\epsilon)$ are Fermi occupation numbers at a small smearing temperature, $|\mathbf{k}, j\rangle$ are the KS states, and the factor 2 accounts for spin. Complex conjugation gives $\chi_{0\mathbf{G},\mathbf{G}'}^*(\mathbf{q},i\omega) = \chi_{0\mathbf{G}',\mathbf{G}}(\mathbf{q},i\omega)$, hence also $\epsilon_{\mathbf{G},\mathbf{G}'}$ is a Hermitian matrix for purely imaginary frequencies. For $\omega \neq 0$, $\mathbf{q} = \mathbf{0}$ and \mathbf{G} or \mathbf{G}' equal to $\mathbf{0}$, this expression vanishes exactly because of orthogonality ($j \neq j'$ terms) or equality of Fermi numbers ($j = j'$). The rate at which χ_0 vanishes as $\mathbf{q} \rightarrow \mathbf{0}$ is relevant for contrasting the Coulomb singularity that appears in the dielectric matrix. To take care of interband terms ($j \neq j'$), a standard solution is to expand the matrix elements of Eq. (13) by means of the formula [26]:

$$\langle \mathbf{k}, j | e^{-i\mathbf{q}\cdot\hat{\mathbf{r}}} | \mathbf{k} + \mathbf{q}, j' \rangle \underset{\mathbf{q} \rightarrow \mathbf{0}}{\simeq} \frac{\langle \mathbf{k}, j | +i\mathbf{q} \cdot \nabla_{\mathbf{r}} | \mathbf{k}, j' \rangle + \langle \mathbf{k}, j | [V_{NL}, i\mathbf{q} \cdot \hat{\mathbf{r}}] | \mathbf{k}, j' \rangle}{\epsilon_{j'}(\mathbf{k}) - \epsilon_j(\mathbf{k})}, \quad (14)$$

where V_{NL} is the non local part of the pseudopotential. By substituting this expansion into Eq. (13) one gets a small \mathbf{q} expansion of the polarizability, which can be used to evaluate the $\mathbf{q} \rightarrow \mathbf{0}$ limit of $q^{-2}\chi_0(\mathbf{q})$ appearing in Eq. (10) when $\mathbf{G} = \mathbf{G}' = \mathbf{0}$. Intraband terms ($j = j'$) are put to zero. While this method is satisfactory for semiconductors, it gives rise to substantial difficulties for metals, where *intraband* terms are also important. This leads to an incorrect evaluation of the χ_0 contributions in the \mathbf{q} -space region closest to the origin, i.e. at one out of N_{kpt} points of the mesh of \mathbf{q} points. At first sight, as χ_0 enters the calculation of Σ through a N_{kpt} -discretized \mathbf{q} -convolution in reciprocal space, one might think that this single incorrect value should affect the energy corrections $\langle \Sigma - V_{XC} \rangle$, with an error of order N_{kpt}^{-1} . However, the singular behavior of the Coulomb repulsion v_C near $\mathbf{q} = \mathbf{0}$ requires an explicit integration around the singular point, which makes the final outcome sensitive to the incorrect $\chi_{0\mathbf{0},\mathbf{0}}(\mathbf{0},i\omega)$ with an error of order $N_{\text{kpt}}^{-\frac{1}{3}}$.

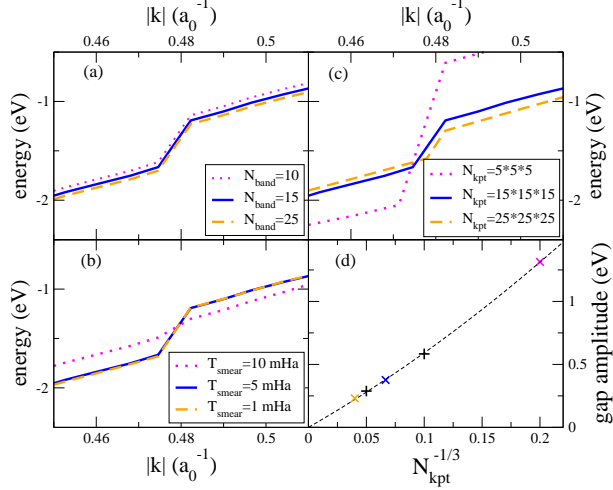


Figure 1: (Color online) G_0W_0 band structure of Na (110 direction), showing the appearance of an unphysical gap, and its dependence on different numerical convergence parameters. Panel (a) shows the dependence with respect to the number of empty states in Eq. (13); (b) with respect to the smearing temperature; (c) with respect to the \mathbf{k} -point mesh. Panel (d) shows the dependence of the unphysical gap on the inverse number of \mathbf{k} -points in each direction; the dashed line is a fitted $a_1 N_{\text{kpt}}^{-1/3} + a_2 N_{\text{kpt}}^{-2/3}$.

III. NAIVE APPLICATION OF A STANDARD G_0W_0 CODE TO METALLIC SYSTEMS

The incorrect small- \mathbf{q} values of χ_0 induce the opening of an unphysical gap at the Fermi energy in the G_0W_0 band dispersion of simple metals (such as the HEG and sodium), as shown in Fig. 1. The figure also shows the convergence properties of the width of this unphysical gap, computed by extrapolation from the two sides. The only significant dependency is on the number N_{kpt} of sample points in the \mathbf{k} -space mesh: Fig. 1 shows that the unphysical gap does tend to close for increasing mesh size, but only extremely slowly, as $N_{\text{kpt}}^{-1/3}$, for the reasons discussed at the end of Sec. II. Therefore, it is practically impossible to close the gap by brute-force mesh refinement, especially because the computation time of the dielectric matrix grows as N_{kpt}^2 .

The spurious gap is essentially independent of most numerical convergence parameters, such as the number of empty states and the smearing temperature, as shown in Fig. 1(a,b). A larger smearing temperature for electronic occupancy would reduce this unphysical gap, but

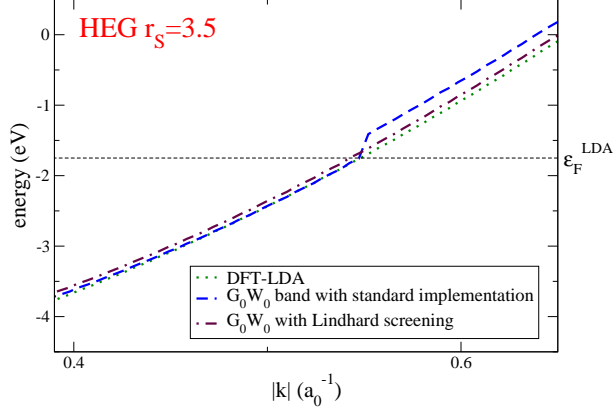


Figure 2: (Color online) Bandstructure for the HEG ($r_s = 3.5 a_0$) computed with the standard implementation of the G_0W_0 method (dashed line). The spurious gap, caused by the lack of the intraband term in the screening, is removed when the computed polarizability is replaced by the Lindhard one (dot-dashed line). The KS band is also displayed for reference (dotted line).

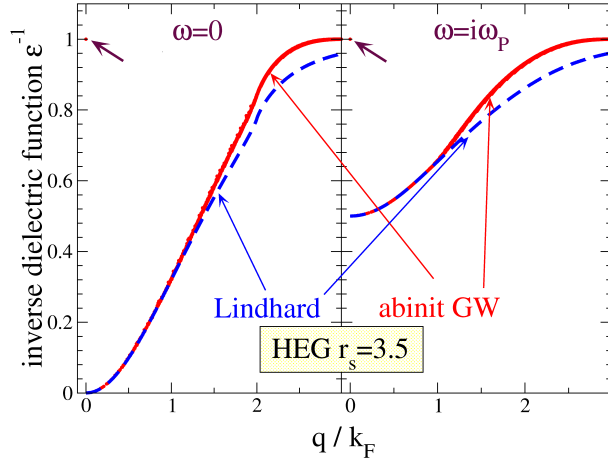


Figure 3: (Color online) Numerically computed HEG screening function $\epsilon^{-1}(\mathbf{q}, \omega)$ ($r_s = 3.5 a_0$), for $\omega = 0$ and $\omega = i\omega_P$, compared to the Lindhard function. For $\mathbf{q} \rightarrow 0$ the discontinuously incorrect points –pointed at by arrows– appear, due to the lack of the intraband term. The differences at large \mathbf{q} are due to the finite number of empty states included in the sums of Eq. (13).

it is a mere technical device, and convergence should be checked in the limit of vanishingly small smearing, where the actual metallic state is recovered.

The origin of the unphysical gap is the incorrect $\mathbf{q} = \mathbf{0}$ value of the screening function as demonstrated in Fig. 2, where the gap is shown to disappear when the numerical dielectric matrix is replaced by the Lindhard function [27]. In metals, the dielectric function ϵ is

expected to diverge when both $\omega \rightarrow 0$ and $\mathbf{q} \rightarrow \mathbf{0}$ (by contrast, it goes to its finite static limit in semiconductors and insulators). For example for the HEG, interband transitions do not contribute to the sum in Eq. (13). At the same time, expression (14) cannot yield correct intraband ($j = j'$) contributions for $\mathbf{q} = \mathbf{0}$, and in practice standard codes do not evaluate such terms due to the equality of the occupancy factors. The resulting incorrect null value of $\chi_0(\mathbf{q} \rightarrow \mathbf{0}, i\omega)$ yields $\epsilon^{-1}(\mathbf{q} \rightarrow \mathbf{0}, i\omega) = 1$, rather than the correct $\epsilon^{-1}(\mathbf{q} \rightarrow \mathbf{0}, i\omega) = \frac{\omega^2}{\omega^2 + \omega_p^2}$, as shown in Fig. 3 where numerical results are compared with the Lindhard function.

A similar discontinuity in G_0W_0 corrections occurs for real metals such as Na and Al. Differently from the HEG, we find $\epsilon^{-1}(\mathbf{0}, i\omega) < 1$, due to the nonzero interband contributions [28]. In particular we obtain $\epsilon_{\text{Na}}^{-1}(\mathbf{q} = \mathbf{0}, 0) \simeq 0.94$, similar to the incorrect HEG value, and $\epsilon_{\text{Al}}^{-1}(\mathbf{q} = \mathbf{0}, 0) \simeq 0.008$. The latter nears the proper Drude value, due to a substantial part of the aluminum Fermi surface being very close to a Brillouin-zone boundary, thus putting many of the metallic contributions of Eq. (13) effectively into inter- rather than intra-band terms. For this reason, in the case of Al, the error induced by neglecting the intraband term is so small that the unphysical gap is almost invisible.

IV. EXTRAPOLATED SMALL- \mathbf{q} POLARIZABILITY

The solution we propose in this paper is devised to avoid the explicit (numerically expensive) integration over the Fermi surface that would be required for a straightforward inclusion of the intraband term. We propose to compute the small \mathbf{q} polarizability by a fit of the expected asymptotics. The time-reversal invariance implies the following symmetry of the matrix polarization:

$$\chi_{0\mathbf{G},\mathbf{G}'}(\mathbf{q}, \omega) = \chi_{0-\mathbf{G}',-\mathbf{G}}(-\mathbf{q}, \omega). \quad (15)$$

Therefore, the small- \mathbf{q} expansion of $\chi_{0\mathbf{0},\mathbf{0}}(\mathbf{q}, i\omega)$ includes only even powers. The expansion of the intraband term ($j = j'$) in Eq.(13) is

$$\chi_{0\mathbf{0},\mathbf{0}}^{intra}(\mathbf{q}, i\omega) \approx \frac{2}{V_{BZ}} \sum_j \int d^3k \delta(\mu - \epsilon_j(\mathbf{k})) \frac{\mathbf{q} \cdot \nabla_{\mathbf{k}} \epsilon_j}{i\omega - \mathbf{q} \cdot \nabla_{\mathbf{k}} \epsilon_j} |1 + \mathbf{q} \cdot \langle \mathbf{k}, j | \nabla_{\mathbf{k}} - i\mathbf{r} | \mathbf{k}, j \rangle|^2. \quad (16)$$

The diagonal matrix element in Eq. (16) is purely imaginary, therefore the last factor is 1 plus a \mathbf{q} -quadratic contribution. For $\omega = 0$ the intraband term is then a constant proportional to the density of states at the Fermi energy, plus quadratic corrections. For $\omega \neq 0$ the term

linear in \mathbf{q} cancels because $\nabla_{\mathbf{k}}\epsilon_j$ is odd and the integral vanishes: the expansion begins with quadratic terms. The expansion of the interband $j \neq j'$ term is easily seen to be no less than quadratic. To sum up, we use the following expression:

$$\chi_{0\mathbf{0},\mathbf{0}}^{\text{fit}}(\mathbf{q}, \omega) = A^\omega + \sum_{rs} B_{rs}^\omega q_r q_s, \quad (17)$$

where A^ω , B_{rs}^ω are real adjustable parameters, and $A^{i\omega_P} = 0$ for $\omega = i\omega_P$. The matrices B^ω are symmetric, and may have further symmetries depending on the crystal geometry.

The off-diagonal elements $\mathbf{G} = \mathbf{0}$ $\mathbf{G}' \neq \mathbf{0}$ of χ_0 (the so-called ‘‘wings’’ of the matrix) are affected by a similar error, since they also contain the contributions of Eq. (14). We also fit the intraband contribution to

$$\chi_{0\mathbf{0},\mathbf{G}'}^{\text{fit}}(\mathbf{q}, \omega) = C^{\omega \mathbf{G}'} + \sum_r D_r^{\omega \mathbf{G}'} q_r, \quad (18)$$

where $C^{\omega \mathbf{G}'}$, $D_r^{\omega \mathbf{G}'}$ are complex adjustable parameters, and $C^{i\omega_P \mathbf{G}'} = 0$ for $\omega = i\omega_P$.

V. RESULTS

We determine the parameters A^ω , B_{rs}^ω , $C^{\omega \mathbf{G}'}$, and $D_r^{\omega \mathbf{G}'}$ in Eqs. (17) and (18) by a standard linear regression on values $\chi_{0\mathbf{0},\mathbf{0}}(\mathbf{q}, \omega)$ and $\chi_{0\mathbf{0},\mathbf{G}'}(\mathbf{q}, \omega)$ computed for nonzero \mathbf{q} -points inside a sphere of radius q_c centered in Γ . We implement this procedure within the `abinit` [12, 18] package. To test the effectiveness of the method, we apply it to the HEG in a simple cubic cell geometry, and to bulk sodium and aluminum in their experimental crystal structures (bcc $a = 8.107 a_0$, and fcc $a = 7.652 a_0$, respectively).

Figure 4 displays the fitting of the computed polarizability χ_0 of the HEG. Panels (a) and (b) compare the computed χ_0 and its small- \mathbf{q} fitted parabolic expansion, for two different cut-off radii q_c . Panels (c)-(f) display the resulting extrapolated small- \mathbf{q} values of the polarizability as functions of the main parameters involved in the simulations and the fit. In these fits, the cut-off radius q_c cannot be chosen too small, or else the number of \mathbf{q} -points becomes insufficient to perform a reliable fit, especially at $\omega = 0$, where the computed χ_0 is affected by significant numerical noise. Likewise, if q_c is increased so much that it becomes comparable with the Fermi momentum k_F , the outer points introduce a systematic error due to the non-parabolic \mathbf{q} -dependency of χ_0 . An intermediate reasonably selected q_c must then be adopted. This is slightly more important for $\omega = i\omega_P$, where the fit is comparably more

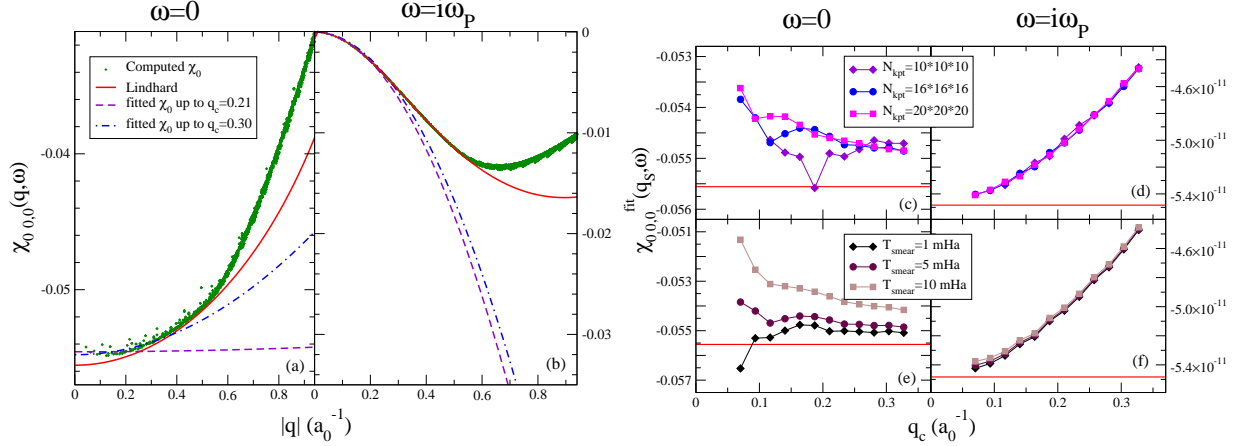


Figure 4: (Color online) The parabolic polarizability χ_0^{fit} , Eq. (17), fitted to the computed $\chi_{00,0}(\mathbf{q}, \omega)$ of the HEG (dots) restricted to \mathbf{q} -points within in a sphere of radius q_c centered at $\mathbf{q} = \mathbf{0}$, and compared to the computed polarizability itself and to the exact (Lindhard) function, for (a) $\omega = 0$ and (b) $\omega = i\omega_P$. The computation involves a cut-off energy of 3 Ha, $N_{\text{kpt}} = 16 \times 16 \times 16$ and a smearing temperature $T_{\text{smear}} = 0.005$ Ha. Panels (c)-(f): convergence of the fitted values $\chi_0^{\text{fit}}(\mathbf{q}_s, \omega)$ (where the tiny $\mathbf{q}_s = (7, 14, 21) 10^{-6} a_0^{-1}$) as a function of the cutoff radius q_c , for different \mathbf{k} -points sampling, and with (c) $\omega = 0$ and (d) $\omega = i\omega_P$, and for different smearing temperature, and with (e) $\omega = 0$ and (f) $\omega = i\omega_P$. Horizontal lines: the exact (Lindhard) values.

sensitive to the value of q_c , as shown in Fig 4(d,f). Comparison to the Lindhard function show that this procedure provides a fairly accurate small- \mathbf{q} χ_0 value, within few percent. Small smearing temperature is beneficial to a better accuracy in the determination of the asymptotic small- \mathbf{q} behavior, but increase the numerical noise in the computed χ_0 .

As Fig. 5 shows, the corrected screening successfully closes the unphysical gap. Of course in aluminum, where the fictitious gap is almost invisible, we see no significant difference in the G_0W_0 corrections computed with and without the fit. The resulting curves are not very sensitive to the fit details, such as the value of q_c , or N_{kpt} . For the HEG we can compare the obtained bands with those computed *via* the Lindhard screening: the tiny almost uniform shift is due to the truncation in the number of empty states included in the summations of Eq. (13), which makes screening different in the large- \mathbf{q} region, as illustrated in Fig. 3.

Table I reports the occupied bandwidths of the metals studied in this work compared to previous calculations and experimental values. The comparison with the DFT-LDA values shows the well-known bandwidth reduction. The results for the HEG are close to Hedin's

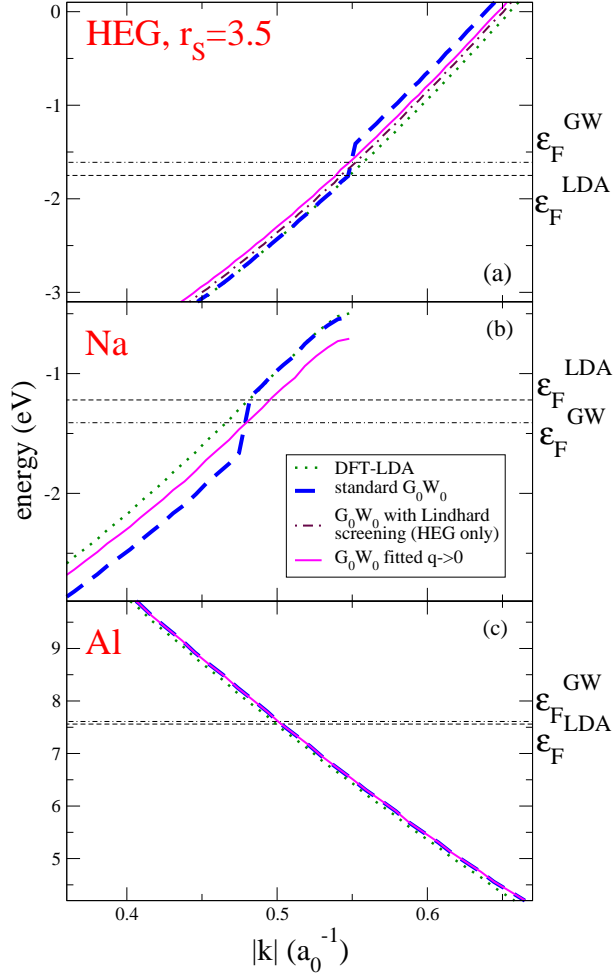


Figure 5: (Color online) Comparison of the band energy obtained via the naive G_0W_0 calculation (dashed) to those obtained with the $\mathbf{q} \simeq 0$ corrected polarizability (solid). For the HEG (a) the figure also shows G_0W_0 results obtained with the analytic (Lindhard) polarizability. For sodium (b) and aluminum (c) the bands are plotted along the (110) and $(11\bar{1})$ directions, respectively.

computations [1], while in the case of Na and Al the numerical values are comparable with data in the literature [29] and approach the experimental values.

VI. CONCLUSIONS

In this work we have shown that the standard G_0W_0 implementation of calculation of quasiparticle-corrected bandstructures, a basic tool to account for weak correlations in semiconductors and insulators, describes metals correctly only in exceptional cases, like Al, where a substantial part of the Fermi surface falls very close to a Brillouin zone boundary, hence

Table I: Occupied bandwidth for the metals studied in this paper. The present results are compared to similar calculations and experimental data. For the HEG, the DFT-LDA result coincides with the free-electron model Fermi energy $\mathcal{E}_F = E_{\text{Ha}} (9\pi/4)^{2/3} (r_s/a_0)^{-2}$. All energies are in eV.

		HEG		Na	Al
r_s/a_0	3	3.5	4	3.93	2.07
DFT-LDA	5.57	4.09	3.13	3.15	11.01
HEG G_0W_0 ^a	5.24	-	2.86	-	-
G_0W_0 for metals ^b	-	-	-	2.52	10.0
present work	5.14	3.84	2.86	2.81	10.03
experiment	-	-	-	2.65 ^c	10.6 ^d

^aCalculations by Hedin [1].

^bCalculations by Northrup *et al.* [29].

^cExperiment by Lyo and Plummer [30].

^dExperiment by Levinson *et al.* [31].

interband contributions make up for the missing intraband screening. In general (like in the HEG and Na), the incorrect intraband contribution to the small- \mathbf{q} screening induces the opening of an unphysical gap at the Fermi energy.

The proposed solution recovers the correct $\mathbf{q} \rightarrow 0$ polarizability by fitting a few small- \mathbf{q} computed values, and solves this difficulty: the gap disappears, and the electron effective mass shows the expected few percent increase. This method requires a negligible computational cost, contrary to other solutions based on Fermi-surface mapping.

An entirely different solution can be devised, which avoids the limitations of the expansion (14), and requires no fit altogether. Since the small- \mathbf{q} polarizability needs to be computed at a \mathbf{q}_s much smaller than those generated by any practical \mathbf{k} -sampling, it is possible to solve the KS equations on *two* \mathbf{k} -point meshes shifted from one another by \mathbf{q}_s , and then apply directly Eq. (13). We tried this method for Na and for the HEG, and find that the typical accuracies practically achievable in KS eigenvalues and wavefunctions allow us to compute χ_0 only for moderately large $|\mathbf{q}|$, of the order of few percent of the \mathbf{k} -mesh spacing. The use of such a not-so-small \mathbf{q}_s as a representative of the $\mathbf{q} \rightarrow \mathbf{0}$ limit would induce systematic errors in the calculation of the G_0W_0 corrections. The fit method is therefore practically

preferable.

Acknowledgments

The authors acknowledge S. Caravati for providing the routines for simulating the HEG within `abinit`. They also thank G. P. Brivio, R. Del Sole, P. Garcia-Gonzales, M. Gatti, R. W. Godby, V. Olevano, L. Reining, F. Sottile, and M. Verstraete for useful discussion. This work was funded in part by the EU's 6th Framework Programme through the NANOQUANTA Network of Excellence NMP4-CT-2004-500198.

-
- [1] L. Hedin, Phys. Rev. **139**, A796 (1965).
 - [2] L. Hedin and S. Lundqvist, in *Solid State Physics*, edited by F. Seitz, D. Turnbull, and H. Ehrenreich (Academic Press, New York, 1969), p. 1.
 - [3] R. W. Godby, M. Schlüter, and L. J. Sham, Phys. Rev. B **37**, 10159 (1988).
 - [4] M. S. Hybertsen and S. G. Louie, Phys. Rev. B **34**, 5390 (1986).
 - [5] M. M. Rieger, L. Steinbeck, I. D. White, H. N. Rojas, and R. W. Godby, Comp Phys. Comm. **117**, 211 (1999).
 - [6] G. Onida, L. Reining, R. W. Godby, R. Del Sole, and W. Andreoni, Phys. Rev. Lett. **75**, 818 (1995).
 - [7] L. Reining, G. Onida, and R. W. Godby, Phys. Rev. B **56**, R4301 (1997).
 - [8] M. Rohlfing, P. Krüger, and J. Pollmann, Phys. Rev. B **48**, 17791 (1993).
 - [9] M. Palumbo, R. Del Sole, L. Reining, F. Bechstedt, and G. Cappellini, Solid State Comm. **95**, 393 (1995).
 - [10] S. Massidda, A. Continenza, M. Posternak, and A. Baldereschi, Phys. Rev. B **55**, 13494 (1997).
 - [11] J. A. Soininen, J. J. Rehr, and E. L. Shirley, J. Phys.: Condens. Matter **15**, 2573 (2003).
 - [12] <http://www.abinit.org/>.
 - [13] <http://www.sax-project.org/>.
 - [14] <http://www.fisica.uniroma2.it/~self/>.
 - [15] E. G. Maksimov, I. I. Mazin, S. N. Rashkeev, and Y. A. Uspensky, J. Phys. F: Met. Phys. **18**, 833 (1988).

- [16] K.-H. Lee and K. J. Chang, Phys. Rev. B **49**, 2362 (1994).
- [17] A. Marini, G. Onida, and R. Del Sole, Phys. Rev. B **64**, 195125 (2001).
- [18] X. Gonze, G. M. Rignanese, M. Verstraete, J. Beuken, Y. Pouillon, R. Caracas, F. Jollet, M. Torrent, G. Zerah, M. Mikami, et al., Zeit. Kristall. **220**, 558 (2005).
- [19] F. Bruneval, N. Vast, and L. Reining, Phys. Rev. B **74**, 045102 (2006).
- [20] B. Holm and U. von Barth, Phys. Rev. B **57**, 2108 (1998).
- [21] W.-D. Schöne and A. G. Eguiluz, Phys. Rev. Lett. **81**, 1662 (1998).
- [22] G. D. Mahan and B. E. Sernelius, Phys. Rev. Lett. **62**, 2718 (1989).
- [23] E. L. Shirley, Phys. Rev. B **54**, 7758 (1996).
- [24] S. L. Adler, Phys. Rev. **126**, 413 (1962).
- [25] N. Wiser, Phys. Rev. **129**, 62 (1963).
- [26] M. S. Hybertsen and S. G. Louie, Phys. Rev. B **35**, 5585 (1987).
- [27] G. D. Mahan, *Many Particle Physics* (Plenum, New York, 1981).
- [28] Interband contributions are identically zero in the HEG.
- [29] J. E. Northrup, M. S. Hybertsen, and S. G. Louie, Phys. Rev. B **39**, 8198 (1989).
- [30] I.-W. Lyo and E. W. Plummer, Phys. Rev. Lett. **60**, 1558 (1988).
- [31] H. J. Levinson, F. Greuter, and E. W. Plummer, Phys. Rev. B **27**, 727 (1983).